Micromagnetic simulation of the temperature dependence of the switching energy barrier using string method assuming sidewall damages in perpendicular magnetized magnetic tunnel junctions

Cite as: AIP Advances **10**, 075106 (2020); https://doi.org/10.1063/5.0007499
Submitted: 29 March 2020 . Accepted: 14 June 2020 . Published Online: 02 July 2020

Hiroshi Naganuma, Hideo Sato, Shoji Ikeda, and Tetsuo Endoh

Micromagnetic simulation of the temperature dependence of the switching energy barrier using string method assuming sidewall damages in perpendicular magnetized magnetic tunnel junctions

Cite as: AIP Advances 10, 075106 (2020); doi: 10.1063/5.0007499
Submitted: 29 March 2020 • Accepted: 14 June 2020 •
Published Online: 2 July 2020

Hiroshi Naganuma,[1,2,3,a)] Hideo Sato,[1,2,3] Shoji Ikeda,[1,2,3] and Tetsuo Endoh[1,2,3,4,5]

AFFILIATIONS

[1]Center for Innovative Integrated Electronic System (CIES), Tohoku University, 468-1, Aoba, Aramaki, Aoba-ku, Sendai 980-8572, Japan
[2]Center for Spintronics Research Network (CSRN), Tohoku University, 2-1-1, Katahira, Aoba-ku, Sendai 980-8577, Japan
[3]Center for Science and Innovation in Spintronics (CSIS), Tohoku University, 2-1-1, Katahira, Aoba-ku, Sendai 980-8577, Japan
[4]Graduate School of Engineering, Tohoku University, Sendai 980-8579, Japan
[5]Research Institute of Electrical Communication, Tohoku University, Sendai 980-8577, Japan

[a)]**Author to whom correspondence should be addressed:** naganuma@cies.tohoku.ac.jp

ABSTRACT

The influence of magnetic damages at the sidewall of perpendicular magnetic tunnel junctions (*p*-MTJs), which are the core devices of spin-transfer-torque magnetoresistive random-access memory (STT-MRAM), is discussed based on the thermal stability factor, Δ, double-logarithmic plot of normalized switching energy barrier, *E*, and saturation magnetization, M_s, and their exponential slope, *n*. Δ was calculated using the string method under the simulation conditions of domain wall motion switching. *n* increased with the increasing thickness of the damaged layer of the sidewall. Notably, the sidewall damage can be explained by the reduction in M_s and exchange stiffness constant, A_s, rather than the interfacial perpendicular anisotropy. The findings of this study are important for controlling and improving the process damage in the mass production of *p*-MTJs in STT-MRAM.

I. INTRODUCTION

In the last decade, considerable effort has been dedicated to developing spintronics-based integrated circuits (ICs) with perpendicular magnetized magnetic tunnel junctions (*p*-MTJs) using interfacial perpendicular magnetic anisotropy (IPA)[1] and Δ_1-coherent tunneling technology.[2–5] They offer high performance at low operation voltage, high endurance, and low power consumption owing to their non-volatile nature.[6] Currently, spintronics-based ICs using spin-transfer-torque[7] magnetoresistive random-access memories (STT-MRAMs) are about to enter into the mass production phase. With these features, spintronics-based ICs can be applied in a variety of applications, such as non-volatile microcontrollers.[8] In general, STT-MRAM in ICs must operate in a specific temperature range, e.g., from −40 °C to 150 °C for grade 1 of automotive application, and also it is necessary to withstand a temperature of 260 °C when the reflow soldering process is used to attach chips to a printed circuit board.[9] Hence, this means that it is important to understand how the performance metrics of the spintronics-based ICs vary with temperature. The thermal stability factor, $\Delta = E/k_BT$, where E is the energy barrier, k_B is the Boltzmann constant, and T is the absolute temperature, is one of the most important performance

metrics as it determines the retention time of given bits in STT-MRAM. Because magnetic properties that determine E in Δ are dependent on temperature, the manner by which E scales with temperature should be elucidated. Generally, two different magnetization reversal modes dominate E, depending on the size of the p-MTJ: one is the domain wall propagation model, and the other is the coherent magnetization reversal model.[10,11] However, E cannot be experimentally explained[12,13] although the decrease in E has been taken into consideration both domain wall propagation and coherent reversal model. Accordingly, the scaling down of E in the experiment may be considered another effect, such as the damaged layer at the sidewall during the microfabrication process.[14,15] If there is no detailed information on "what kind of damaged layer is formed," IC design cannot be performed precisely. Detailed information on the damaged layer thickness and degradation of M_s, magnetic anisotropy, A_s, and Δ is difficult to understand using mere experimental data. Many reports are available on micromagnetic simulations because a simulation method can individually set damaged information.[16–18] A few studies have used the temperature dependence of Δ and magnetic properties of the damaged layer to reproduce experimental data. Thus, we think that it is important to deeply understand the temperature dependence of Δ, including the damaged layer, to develop STT-MRAMs for industrial applications, such as automobiles and social infrastructure, where guaranteeing safety operation at high temperatures is required. In this study, a micromagnetic simulation based on the string method is used to calculate the temperature dependence of Δ using various types of magnetic parameters and reproduce the temperature dependence of Δ and magnetic properties in the experimental data of previously reported p-MTJs.[13]

II. THEORY

Δ and the switching mode of magnetization are strongly dependent on magnetic materials. High-crystalline magnetic anisotropy materials, such as $L1_0$-ordered alloys,[19] are attractive from the viewpoint of thermal stability with large Δ. Because IPA in CoFeB/MgO is compatible with Si-based CMOS technology, the magnetic properties used here for calculations refer the CoFeB/MgO system. Here, the ideal temperature dependence of E for p-MTJs with the CoFeB/MgO system based on the two reversal models is described. The domain wall propagation model is observed at a large size of p-MTJs down to a critical p-MTJ size, below which the coherent magnetization reversal model is observed. For the domain wall propagation model, E is expressed as $E = 4(A_s K_{eff})^{0.5} Dt$, and for the coherent magnetization reversal model, $E = K_{eff} t\pi\left(\frac{D}{2}\right)^2$, where K_{eff} is the effective perpendicular magnetic anisotropy energy density, t is the free layer thickness, and D is the diameter of the circular p-MTJs. In these formulas, A_s and K_{eff} are the two relevant magnetic properties determining E. The temperature dependence of A_s and K_{eff} is correlated with that of M_s through a power-law scaling relationship,

$$\frac{A_s(T)}{A_s(T^*)} = \left\{\frac{M_s(T)}{M_s(T^*)}\right\}^2, \tag{1}$$

$$\frac{K_{eff}(T)}{K_{eff}(T^*)} = \left\{\frac{M_s(T)}{M_s(T^*)}\right\}^{\sim 2}, \tag{2}$$

where T^* is the normalizing temperature at 0 K. The power-law scaling for the temperature dependence of A_S was reported in Ref. 20. K_{eff} of the CoFeB/MgO system can be expressed as $K_{eff}(T) = K_i + \left(K_b - \frac{(M_s)^2}{2\mu_0}\right)$, where K_i is the interfacial anisotropy at the CoFeB/MgO system, and K_b is the bulk magnetic anisotropy energy density. Because the contribution of K_b to K_{eff} is negligibly small and the T dependence of K_i is correlated with that of M_s through the power-law scaling with an exponent of approximately 2,[21,22] the exponent for the T dependence of K_{eff} should also be around 2. From these relationships, one can derive the following scaling relationships between the T dependencies of E and M_s, which is independent of the reversal model,

$$\frac{E(T)}{E(T^*)} = \left\{\frac{M_s(T)}{M_s(T^*)}\right\}^{\sim 2}. \tag{3}$$

Although the value of the exponent is expected to be approximately 2, the experimentally determined value was much larger than 2 and ranged from 3 to 5.[13] One possible reason for the discrepancy can arise from the finite damage on the sidewall of the p-MTJ during device processing in the experiment.

III. METHODS

The energy barrier was calculated by the micromagnetic simulator EXAMAG[23] incorporating the string method. The string method[24–26] is useful in identifying the minimum energy path between the parallel (P) and antiparallel (AP) states of MTJs. The magnetic energy states of the demagnetization energy for z axis E_d, anisotropy energy, E_{ani}, exchange energy, E_{exc}, and total energy, E_{all}, are calculated in each point in the free energy landscape between bistable states. $\vec{a}_1$ and K_U are the unit vector of the magnetic easy axis and the uniaxial magnetocrystalline anisotropy constant, respectively. The energy states are described as follows:

$$E_d(\vec{M}) = -\frac{1}{2}\vec{M}\cdot\vec{H}, \tag{4}$$

$$E_{ani}(\vec{M}) = -\frac{K_U}{M_S^2}(\vec{a}_1\cdot\vec{M})^2, \tag{5}$$

$$E_{exc}(\vec{M}) = \frac{A_S}{M_S^2}\left\{(\vec{\nabla}M_x)^2 + (\vec{\nabla}M_y)^2 + (\vec{\nabla}M_z)^2\right\}, \tag{6}$$

$$E_{all} = \int dV\{E_{ani} + E_{exc} + E_d\}. \tag{7}$$

A few studies investigated and calculated that E and Δ have sidewall damages.[16] However, a full stacking structure is necessary in applications because such a structure can consider the influence of a stray field and exchange coupling in each layer.[27] Subsequently, the model of the stacking structure was a full stacking p-MTJ structure referenced from an experimental report[17] [Fig. 1(a)]. The junction diameter and the sidewall angle were 30 nm and 87.5°, respectively. The damaged layer was formed on the sidewall of the dot with a uniform thickness, and the diameter, including the damaged layer, was fixed at 30 nm [Fig. 1(b)]. The thickness of the damaged layer was 1 nm, 3 nm, 5 nm, and 7 nm. The magnetic parameters, M_s,[13] perpendicular magnetic anisotropy H_k,[28] and A_s,[29,30] used in the calculation, were referred from the experimental results [Fig. 1(c)]. A

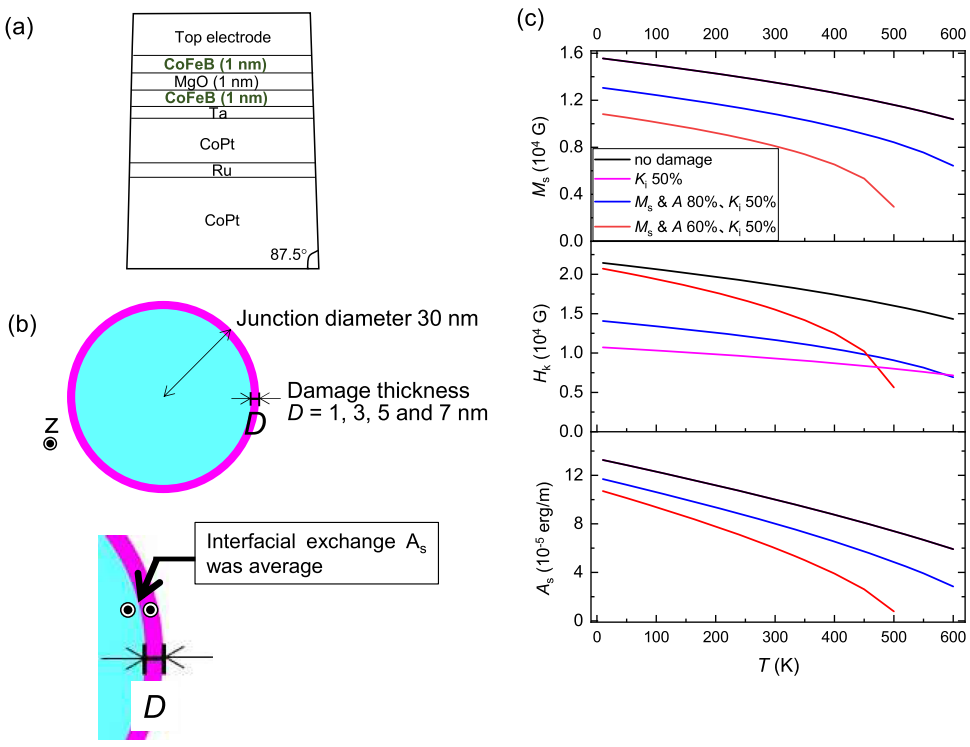

FIG. 1. (a) Stacking structure of *p*-MTJs, (b) junction diameter of 30 nm and damaged layer formed at the sidewall of the dot (d = 1 nm, 3 nm, 5 nm, and 7 nm), and (c) temperature dependence of magnetic parameters, M_s, A_s, and H_k, for simulation.

part of these magnetic parameters were obtained from the film form, which is based on the fabrication process of an STT-MRAM on a 300 mm wafer. The decrease in H_k was caused by the physical damage at the CoFeB/MgO interface. As such, the damages occurred during ion etching in the microfabrication process, and no change was found in the Curie temperature. The decrease in M_s and A_s may be caused by the inclusion of different atoms due to the chemical processes during microfabrication, and the Curie temperature was decreased. So, the process damage can be visualized by comparing the calculation and experimental results. Because H_k, M_s, and A_s are related to one another in actual magnetic materials, the changes in H_k, M_s, and A_s may not be completely independent. Therefore, the magnetic parameters in the calculation were utilized to stand out as possible as actual magnetic materials. Three different types of damage were assumed: (i) 50% of reduced H_k, (ii) 50% of reduced H_k and 20% of reduced M_s and A_s, and (iii) 50% of reduced H_k and 40% of reduced M_s and A_s. These magnetic parameters were set as the reference and recording layers. A_s at the interface of the sidewall was set as the average of the damaged and no-damage values. The units used in this study are based on cgs.

IV. SIMULATION RESULTS AND DISCUSSION

To reduce the total calculation cost, the magnetization curves (M–H) were simulated before the calculation of E, and we only calculated the minimum energy path from the P to AP state. Figure 2 shows the M–H curves of the no-damage and 3-nm-thick damaged *p*-MTJs. M_s and coercivity were decreased by the damage, and the amount of the reduction of coercivity depended on the type of damage. Figures 3(a) and 3(d)–3(f) show the magnetic parameters of E_d, E_{ani}, E_{exc}, and E_{all} during the paths' minimum motions between bistable states. The calculation is based on Eqs. (4)–(7). $\vec{H}$ is the static magnetic field vector, and $\vec{M}$ is the magnetization vector. E_{all} can be described by the summation of each energy. The Zeeman energy was not included because the external magnetic field is not applied in the

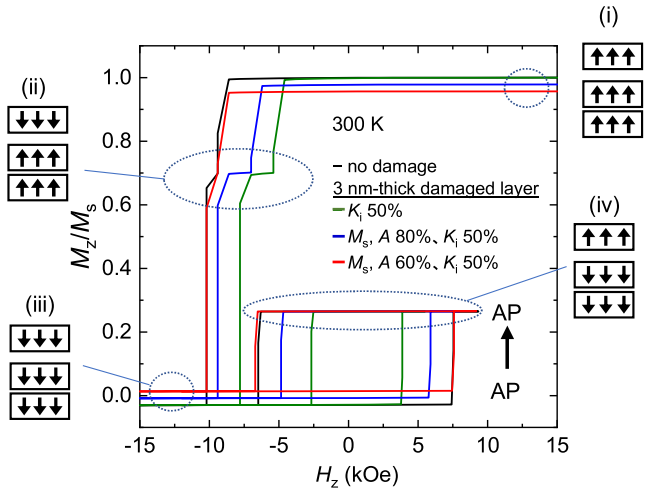

FIG. 2. Normalized perpendicular magnetization (M_z/M_s) vs magnetic field (H_z) curves at 300 K for the *p*-MTJs with various damaged parameters.

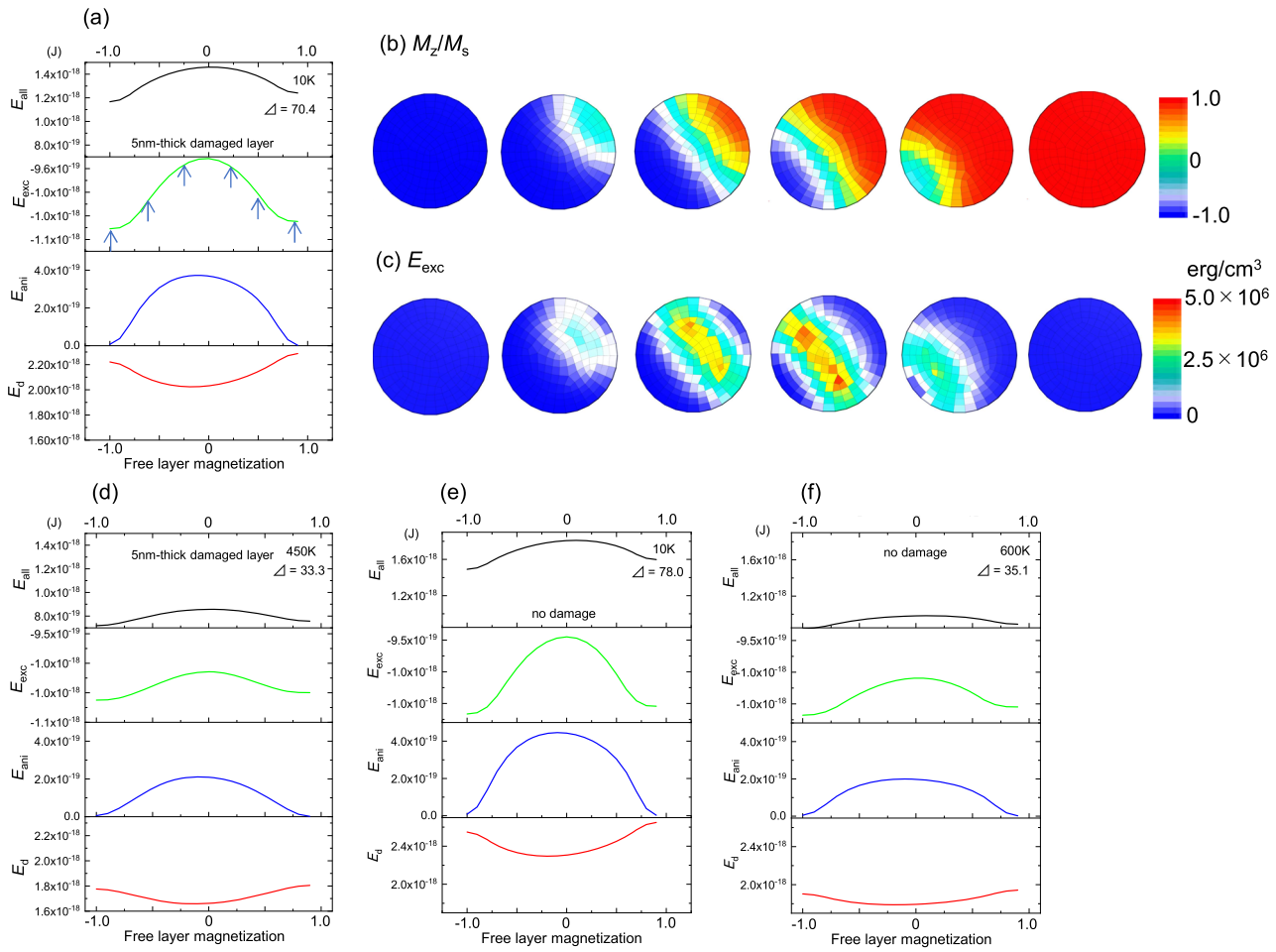

FIG. 3. Demagnetization energy, E_d, anisotropy energy, E_{ani}, exchange energy, E_{exc}, and total energy, E_{all} during the pathing minimum route for switching by the string method. [(a) and (d)] 5-nm-thick damaged layer with the magnetic parameters of 50% of reduced H_k and 40% of reduced M_s and A_s at 10 K and 450 K; [(b) and (c)] domain mapping of normalized perpendicular magnetization (M_z/M_s) and E_{exc} corresponding to the damaged case described in Fig. 1(b); [(e) and (f)] no damaged dot at 10 K and 600 K.

case of the string method. E_d, E_{ani}, and E_{exc} are the total energy of the full stacking of *p*-MTJs, and the corresponding domain images are the energies of each layer. The interlayer coupling of Ru also includes the curves of E_{exc}. E_{exc} was at maximum at the antiparallel spin configuration and minimum in the parallel spin configuration, and these values are always positive due to the sign of A_s. The vertical axis of the curves represents the energy, and the E_{exc} domain mappings are represented as erg/volume. Here, in the case of the E_{exc} curve, the sign of E_{exc} is negative because E_{exc} is the summation of the total layer. Figures 3(b) and 3(c) show the mapping images of the normalized magnetization, M_z/M_s, and E_{exc} component, respectively. Each mapping image is presented as arrows in Fig. 3(a). M_z/M_s is aligned to the perpendicular direction in each bistable state. Figure 3(a) shows the results for the 5-nm-thick damaged layers with the damaged magnetic parameters of (iii) at 10 K. The cause of the asymmetric curve energy profiles is the influence of the stray field from the reference layer. E_{all}, E_{exc}, and E_{ani} show an upward convex curve, and E_d shows a downward convex curve. The domain images of M_z/M_s and E_{exc} showed the change in contrast during switching, which corresponds to the maximum point of E_{exc} in Fig. 3(a). These results indicate the formation of the domain wall during the energy path. The relative angle of magnetization increased with the formation of the domain wall at the saddle point. The M_z component decreased due to the relative angle of spins; therefore, E_d becomes the smallest when E_{exc} is the maximum. E_{all} decreased when the temperature increased to 450 K [Fig. 3(d)] due to the decrease in the base energy level E_d, which indicates the decrease in the magnetostatics energy. In the case of E_{exc} at 450 K, the domain wall still exists at the saddle point. Figures 3(e) and 3(f) show the energy profiles at 10 K and 600 K for the *p*-MTJs without the damaged layer. The domain wall was also formed in the *p*-MTJs without the damaged layer. Although magnetic parameters are slightly different, the condition of the domain wall formation is almost consistent with that of previous results.[27] Δ of the no-damage *p*-MJTs is higher than that of

the damaged *p*-MTJs. All the calculations in this study showed the domain wall motion, and a coherent switching was not observed.

Figure 4(a) shows the energy (E) and Δ (E/k_BT) for the 3-nm-thick damaged *p*-MTJs with damaged parameters of (i)–(iii). The *p*-MTJs without the damaged layer are used as control. The damaged *p*-MTJs show smaller Δ at all temperatures. The damaged parameters (ii) and (iii) were crossover at approximately 450 K, which is attributed to the temperature dependence of H_k [Fig. 1(c)]. In order to estimate the slope with various types of damaged parameters, Eq. (3) was systematically examined for the *p*-MTJs. Figures 4(a) and 4(b) show E(T)/E(10 K) vs M_s(T)/M_s(10 K) and (b) exponent value estimated from E(T)/E(10 K) vs M_s(T)/M_s(10 K). The thickness of the damaged layer was fixed to 3 nm. The exponent for the no-damage *p*-MTJs was approximately 2, which is consistent with that in Eq. (3). In the case of magnetic parameter (i), H_k was reduced to half in the damaged layer. Here, H_k is almost equal to K_i because CoFeB is thin enough and perpendicular magnetic anisotropy (PMA) occurred at the interface between the CoFeB and MgO barriers. The exponent of 50% of K_i was almost the same as that of the no-damage *p*-MTJs. On the contrary, when M_s and A_s were reduced to 80% with a K_i of 50%, the exponent was increased. The exponent was increased to ~2.8 in the case of 60% of M_s and A_s and 50% of K_i. These results indicate that the magnetic parameters of M_s and A_s in the damaged layer clearly showed the differences in the exponent value.

To further understand the damage mechanism, various thicknesses of the damaged layers were systematically investigated. Figures 5(a) and 5(b) show various thicknesses and magnetic parameters for the damaged layer, and Fig. 5(c) shows their exponent. Note that the thicknesses, except 7 nm, had an exponent of approximately 2, with 50% of K_i [magnetic damaged parameter of case (i)]. In the case of damage parameters (ii) and (iii), the exponent increased with the increase in the thickness of the damaged layer. By increasing the damaged layer to 7 nm, the magnetization switching was not a simple bistable state in the M–H curves and magnetization switching through the mixture of perpendicular and in-plane magnetization. Therefore, the minimum energy paths are complicated, and E cannot be decided in this work. Below the thickness of the damaged layer of 5 nm, K_i did not show any differences in the exponent, but M_s and A_s showed evident defenses, and the decrease in these parameters influenced the exponent. Comparing the experimental data of *p*-MTJs (exponent n = 3.1),[13] the simulation data of the 5-nm-thick damaged layer and the damage case of (iii) (exponent n = 3.0) showed almost consistent results. Hence, the type of damage in the experimental case is the impurity atoms that penetrated and diffused into CoFeB and degrade the magnetic parameters of M_s and A_s, rather than the degradation of perpendicular magnetic anisotropy at the interface by physical damage. For the experimental data (n = 3.1),[13] they used reactive ion etching and Ar ion milling as the patterning process for *p*-MTJs. Our

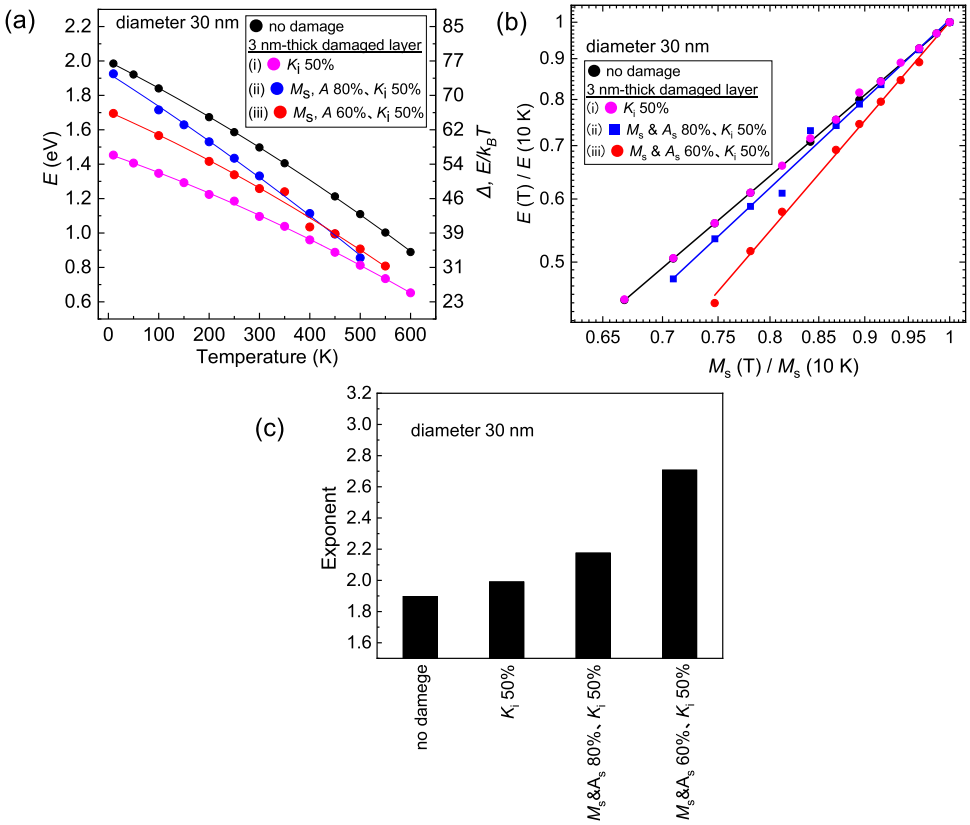

FIG. 4. (a) E and Δ vs temperature, (b) E (T)/E(10 K) vs M_s(T)/M_s(10 K) for various types of damaged *p*-MTJs, and (c) slope estimated from E(T)/E(10 K) vs M_s(T)/M_s(10 K). The junction diameter is 30 nm, which includes the thickness of the damaged layer of 3 nm.

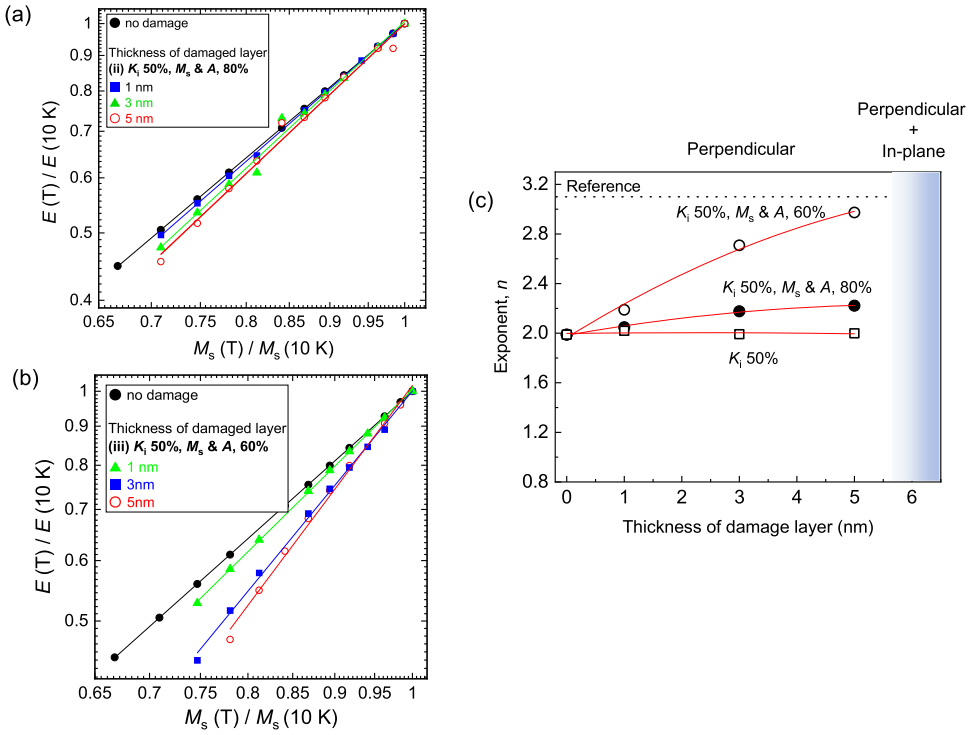

FIG. 5. E(T)/E(10 K) vs M_s(T)/M_s(10 K) of (a) K_i 50%, M_s, A_s 80% and (b) K_i 50%, M_s, A_s 60% for various thicknesses of damaged layers; and (c) thickness dependence of the exponent slopes, n.

calculation was performed by considering the damage in the p-MTJ sidewall. Hence, the assumption is that the other atoms come from the outside of the p-MTJs, and the interdiffusion of each layer was considered. Thus, the process gases, such as nitrogen and hydrogen, used in the microfabrication degrade the magnetic properties of CoFeB. The management of process gases during microfabrication requires additional attention for preparing high-quality p-MTJs integrated to ICs.

V. CONCLUSIONS

The magnetization behavior of p-MTJs was calculated using the string method with various magnetic parameters and thicknesses of damaged layers. During the paths' minimum energy motions, all the p-MTJs formed a domain wall during switching. Considering the double-logarithmic plot of the normalized switching E, M_s, and their exponential slope n, n was strongly influenced by the damage parameters of M_s and A_s. The increase in n in the experiment can be well explained by assuming that the impurities penetrate into the sidewall and formed a damaged layer. The magnetic stability of p-MTJs can be drastically improved by controlling the process gases during microfabrication.

ACKNOWLEDGMENTS

This work was supported by the STT-MRAM R&D program under Industry–Academic collaboration of the CIES consortium. This work was financially supported by JST-OPERA Program Grant No. JPMJOP1611, the Cross-ministerial Strategic Innovation Promotion Program (SIP) by CAO, the Center for Spintronics Research Network (CSRN), and the Center for Science and Innovation in Spintronics (CSIS).

DATA AVAILABILITY

The data that support the findings of this study are available from the corresponding author upon reasonable request.

REFERENCES

[1] S. Ikeda, K. Miura, H. Yamamoto, K. Mizunuma, H. D. Gan, M. Endo, S. Kanai, J. Hayakawa, F. Matsukura, and H. Ohno, Nat. Mater. **9**, 721 (2010).
[2] W. H. Butler, X.-G. Zhang, T. C. Schulthess, and J. M. MacLaren, Phys. Rev. B **63**, 054416 (2001).
[3] J. Mathon and A. Umerski, Phys. Rev. B **63**, 220403 (2001).
[4] S. Yuasa, A. Fukushima, T. Nagahama, K. Ando, and Y. Suzuki, Jpn. J. Appl. Phys., Part 2 **43**, L588 (2003).
[5] S. S. P. Parkin, C. Kaiser, A. Panchula, P. M. Rice, B. Hughes, M. Samant, and S.-H. Yang, Nat. Mater. **3**, 862 (2004).
[6] H. Ohno, T. Endoh, T. Hanyu, N. Kasai, and S. Ikeda, in *IEDM Technical Digest* (IEEE, 2010), pp. 9.4.1–9.4.4.
[7] J. Slonczewski, J. Magn. Magn. Mater. **159**, L1 (1996).
[8] M. Natsui, D. Suzuki, A. Tamakoshi, T. Watanabe, H. Honjo, H. Koike, T. Nasuno, Y. Ma, T. Tanigawa, Y. Noguchi, M. Yasuhira, H. Sato, S. Ikeda, H. Ohno, T. Endoh, and T. Hanyu, IEEE J. Solid-State Circuits **54**, 2991 (2019).
[9] K. Lee, K. Yamane, S. Noh, V. B. Naik, H. Yang, S. H. Jang, J. Kwon, B. Behin-Aein, R. Chao, J. H. Lim, S. K, K. W. Gan, D. Zeng, N. Thiyagarajah, L. C. Goh, B. Liu, E. H. Toh, B. Jung, T. L. Wee, T. Ling, T. H. Chan, N. L. Chung, J. W. Ting, S. Lakshmipathi, J. S. Son, J. Hwang, L. Zhang, R. Low, R. Krishnan, T. Kitamura,

Y. S. You, C. S. Seet, H. Cong, D. Shum, J. Wong, S. T. Woo, J. Lam, E. Quek, A. See, and S. Y. Siah, in *IEEE Symposium VLSI Technol Digest Technical Papers* (IEEE, 2018), p. 183.
[10]E. C. Stoner and E. P. Wohlfarth, Philos. Trans. R. Soc., A **240**, 599 (1948).
[11]G. D. Chaves-O'Flynn, G. Wolf, J. Z. Sun, and A. D. Kent, Phys. Rev. Appl. **4**, 024010 (2015).
[12]J. H. Kim, W. C. Lim, U. H. Pi, J. M. Lee, W. K. Kim, J. H. Kim, K. W. Kim, Y. S. Park, S. H. Park, M. A. Kang, Y. H. Kim, W. J. Kim, S. Y. Kim, J. H. Park, S. C. Lee, Y. J. Lee, J. M. Yoon, S. C. Oh, S. O. Park, S. Jeong, S. W. Nam, H. K. Kang, and E. S. Jung, in *IEEE Symposium VLSI Technol Digest Technical Papers* (IEEE, 2014), p. 76.
[13]E. C. I. Enobio, M. Bersweiler, H. Sato, S. Fukami, and H. Ohno, Jpn. J. Appl. Phys., Part 1 **57**, 04FN08 (2018).
[14]Y. Ohsawa, N. Shimomura, T. Daibou, Y. Kamiguchi, S. Shirotori, T. Inokuchi, D. Saida, B. Altansargai, Y. Kato, H. Yoda, T. Ohkubo, and K. Hono, IEEE Trans. Magn. **52**, 3400803 (2016).
[15]Y. Iba, A. Takahashi, A. Hatada, M. Nakabayashi, C. Yoshida, Y. Yamazaki, K. Tsunoda, and T. Sugii, in *IEEE Symposium VLSI Technol Digest Technical Papers* (IEEE, 2014), p. 74.
[16]K. Song and K.-J. Lee, J. Appl. Phys. **118**, 053912 (2015).
[17]K. Ito, S. Ohuchida, M. Muraguchi, and T. Endoh, Jpn. J. Appl. Phys., Part 1 **54**, 04DM01 (2015).
[18]C. Yoshida, T. Tanaka, T. Ataka, and A. Furuya, IEEE Trans. Magn. **55**, 3401105 (2019).
[19]H. Naganuma, G. Kim, Y. Kawada, N. Inami, K. Hatakeyama, S. Iihama, K. M. N. Islam, M. Oogane, S. Mizukami, and Y. Ando, Nano Lett. **15**, 623 (2015).
[20]C. Herring and C. Kittel, Phys. Rev. **81**, 869 (1951).
[21]H. Sato, P. Chureemart, F. Matsukura, R. W. Chantrell, H. Ohno, and R. F. L. Evans, Phys. Rev. B **98**, 214428 (2018).
[22]J. G. Alazate, P. K. Amiri, G. Yu, P. Upadhyaya, and J. A. Katine, Appl. Phys. Lett. **104**, 112410 (2014).
[23]See http://fujitsu.com/global/about/resources/news/press-releases/2015/0324-01.html for Fujitsu Ltd.
[24]E. Weinan, R. Weiqing, and E. V. Eijnden, Phys. Rev. B **66**, 052301 (2002).
[25]W. E, W. Ren, and E. Vanden-Eijnden, J. Appl. Phys. **93**, 2275 (2003).
[26]L. Maragliano, A. Fischer, E. Vanden-Eijnden, and G. Ciccotti, J. Chem. Phys. **125**, 024106 (2006).
[27]C. Yoshida, T. Tanaka, T. Ataka, J. Fujisaki, K. Shimizu, T. Hirahara, H. Shitara, A. Furuya, and Y. Uehara, Jpn. J. Appl. Phys., Part 1 **58**, SBBB05 (2019).
[28]E. C. I. Enobio, H. Sato, S. Fukami, F. Matsukura, and H. Ohno, IEEE Magn. Lett. **6**, 5700303 (2015).
[29]T. Dohi, S. Kanai, F. Matsukura, and H. Ohno, Appl. Phys. Lett. **111**, 072403 (2017).
[30]N. Ichikawa, T. Dohi, A. Okada, H. Sato, S. Fukami, and H. Ohno, Appl. Phys. Lett. **112**, 202402 (2018).